Chaos, Solitons and Fractals 181 (2024) 114570

Contents lists available at ScienceDirect

Chaos, Solitons and Fractals

journal homepage: www.elsevier.com/locate/chaos

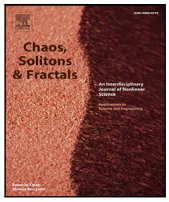

Feedback control of chaos in impact oscillator with multiple time-delays

Dimitri Costa *, Ekaterina Pavlovskaia, Marian Wiercigroch

Centre for Applied Dynamics Research, School of Engineering, University of Aberdeen, King's College, Scotland, Aberdeen AB24 3FX, United Kingdom

ARTICLE INFO

Keywords:
Nonsmooth dynamics
Nonlinear control
Multi-stability
Systems with delay
Floquet theory

ABSTRACT

Extended time-delayed feedback control (ETDF) has emerged as a promising control method for nonlinear systems, with applications in diverse fields such as energy harvesting, vibration mitigation, and chaos control. Whilst novel ETDF-based approaches incorporating multiple periods of a target orbit as time delays have been explored, a comprehensive analysis of the underlying phenomena and limitations of ETDF with such delays is lacking. In this study, we investigate the effects of various delays and the strength of the original instability of the target unstable periodic orbit on ETDF control using experimental data from an impact oscillator. Surprisingly, we observe that ETDF loses its ability to stabilize a target orbit when delays are even multiples of the target orbit's period. By combining Floquet theory, semi-analytical methods, experimental data, and numerical simulations, we unveil the fundamental mechanisms responsible for this loss of efficacy. Specifically, we demonstrate that stability cannot be achieved for delays that are even multiples of the target orbit period due to a shift in the imaginary parts of Floquet exponents as controller gains approach infinity. In contrast, by using odd multiples of the target orbit period as delays a more gradual degradation of stability is observed as their multiplicity increases. Furthermore, we propose a method to predict the maximum instability of an orbit that can be counterbalanced by ETDF. Our findings offer essential insights for the design of robust and efficient control strategies based on ETDF, while advancing our understanding of the underlying mechanisms governing such controllers.

1. Introduction

Time-delayed feedback control (TDF) [1] is a promising family of methods that has the potential to become a widely used standard for some classes of nonlinear systems. Due to their design, they can take advantage of the system dynamics to reduce their energy consumption and the system's knowledge requirements. These attributes have inspired researchers to use TDF to enhance effective range of sea wave energy harvesters [2], to mitigate friction induced vibration [3], to improve the accuracy of atomic force microscopes [4,5], to control spatiotemporal chaos [6], to stabilize the power output of high power lasers [7], to control cardiac rhythms [8] and even to control nonlinear behaviour of agricultural tractors [9].

The origin of TDF can be traced to the seminal work of Pyragas [1, 10], where unstable periodic orbits (UPOs) embedded in a chaotic attractor were stabilized for the first time by a continuous control. Since this pioneering work, several researchers studied TDF control to uncover its limitations and propose innovative modifications to overcome them. A number of contributions has been made including those by Socolar et al. [11] on the idea of using an infinite sum of delayed states as feedback, Lehnert et al. [12,13] by suggesting an adaptive modification through the introduction of controller gains' dynamics, Pyragas and Pyragas [14] proposing an adaptive delay to the control and Pyragas [15] solving the limitations of the original TDF control revealed in [16] by introducing an unstable state to the control. Other modifications utilize periodically varying gains to avoid the same limitation [17–21].

Although originally focused on chaos control, the use of TDF has also expanded to several other scenarios. De Paula et al. [22,23] uses TDF as a bifurcation control to extend the stabilization range of an orbit. Other works focus on the use of TDF methods for the synchronization of nonlinear systems [24,25]. Most recently, Costa et al. [26] proposed to change controller time-delays to switch between co-existing attractors and UPOs in a non-smooth system [27,28]. Their results show that depending on the parity of the division, $j = \tau/\tau_s$, between the control delay, τ, and orbit period, τ_s, the stability of controlled UPO drastically changes. They also proposed a new fractional time-delayed feedback method to switch between a co-existing period-l and period-jl orbits. Other studies also try to explore TDF influence in multi-stability, Zhang et al. [29] analyses TDF influence on basins of attraction and the influence of small variations in delay on the control effectiveness [30]. Although comprehensive in their analysis,

* Corresponding author.
E-mail address: dimitri.costa@abdn.ac.uk (D. Costa).

https://doi.org/10.1016/j.chaos.2024.114570
Received 23 October 2023; Accepted 4 February 2024
Available online 22 February 2024

these works are focused on applications of the TDF control and are based on numerical simulations, without dipping into advanced tolls of stability analysis to explain the origins of the observed phenomena.

Analytical studies of TDF methods and analysis of the complex dynamics occurring during stabilization of controlled orbits is a challenging task. As such, only a few works try to use Lyapunov theory to analyse TDF [31] due to the difficulty in the calculation of Lyapunov exponents in delayed systems. In contrast, the use of Floquet theory to analyse TDF was largely adopted. A series of works discuss the inability of ETDF control to stabilize orbits with an odd number of positive Floquet exponents [16,32,33]. Other work, used Floquet exponents to analyse the influence of ETDF parameters on the target orbit stability in numerical [34–38] and experimental [39,40] studies. Pyragas [41] reviwed several of these studies, and highlighted an equivalence between Floquet exponents of an orbit stabilized by proportional gain control and TDF [35]. However, despite the fact that delayed system usually present multi-stability [42], to the authors' knowledge, there are still no analysis discussing the control effectiveness and underlying phenomena when TDF delays are different from the target orbit. Only an investigation [43] analysing bifurcation diagrams in a limited vicinity of nominal delays was found. In their work, the authors investigate how linear approximations of a parameter dependent period for a typical Hopf bifurcation, influence the controller's effectiveness when used as control delays.

Most recently, the issue of TDF and multi-stability has been reported by Friart et al. [44] discussing the creation of orbits with periods equal to fractions of the delay, whilst Schöll et al. [45,46] analyse how multistability seems to increase as the delay of the controller increases. Another issue was raised by Huang [47] reporting a loss of stability of an orbit after a maximum value of the delay. There is still a lack of explanation for those limitations and how they can be addressed.

Aiming to fill the gap in the analysis of TDF with different delays, we analyse the effects of multiples of the target orbit period as delays and original instability of the target orbit on TDF control and explain the underlying phenomena behind the controller's inability to stabilize its target when using even multiples of the orbit period as delays. We take advantage of an impact oscillator rig capable of testing a wide range of control methods [27,28]. This is crucial for the implementation and understanding of control methods such as the ones proposed in [14,26] and it also enables analysis of their robustness to noise. Our results demonstrate that a sudden instability with even multiples of the target's orbit period as delay is generated by a shift in the imaginary parts of Floquet exponents when gains tend to infinity. We also establish that such shift does not happen for delays that are odd multiples of the orbit period and that stability degrades more gradually for higher multiples. Finally, we propose a novel method to predict the maximum highest real valued Floquet exponent that an uncontrolled UPO can present before the ETDF control is unable to stabilize it. We also test whether the equivalence between proportional feedback and ETDF initially proposed in [36] is also valid for a non-smooth system.

This work is organized as follows. In Section 2, we introduce the impact oscillator experimental setup and its corresponding mathematical model. Afterwards, we numerically explore the dynamics of the model and identify relevant cases for our analysis. Next, we investigate both numerically and experimentally the effects of different delays in the control of an unstable period-1 orbit. In Section 3, we establish the mathematical basis to analyse the control by utilizing Floquet theory and an equivalence between proportional feedback and ETDF as proposed in [36]. In Section 4, we analyse the impact oscillator with the developed mathematical methods and perform a comprehensive parametric analysis between controlled UPO Floquet exponents, controller delay and initial orbit instability. Finally, we summarize our findings and draw conclusions in Section 5.

2. Control of an impact oscillator with multiple delays

The TDF method was originally proposed by Pyragas [1] and later extended by Socolar [11] as the ETDF method. Its main idea is to use a proportional feedback of delayed observations $\mathbf{y}$ to control the dynamical system responses. Thus, the control signal $\mathbf{u}$ of the ETDF method can be expressed as:

$$\mathbf{u} = \mathbf{K}\left((1-r)\left(\sum_{n=1}^{\infty} r^{n-1}\mathbf{y}(t-n\tau)\right) - \mathbf{y}(t)\right), \tag{1}$$

where $\mathbf{K}$ is the gain matrix and r, ranging from 0 to 1, is a control parameter.

Originally, the method only considered stabilization of UPOs, where the delay τ should be equal to the target unstable orbit's period [1]. However, recent studies explored the use of different delays to switch between co-existing attractors, e.g. [26]. Other work [23] highlights a problem as it clains that ETDF can stabilize any orbit that satisfies the equation $\mathbf{y}(t) = \mathbf{y}(t-\tau)$. In other words, ETDF can stabilize a period-l orbit, $l = 1, 2, 3...$, different from the targetted period-jl orbit, $j = 1, 2, 3...$, as system's observations would still obey, due to the periodicity of the system:

$$\mathbf{y}(t) = \mathbf{y}(t - l\tau_1) = \mathbf{y}(t - 2l\tau_1) = \mathbf{y}(t - 3l\tau_1)... = \mathbf{y}(t - jl\tau_1), \tag{2}$$

where $l\tau_1$ is the period of a period-l orbit and τ_1 is the period of a period-1 orbit. In this example, τ is the delay of the controller and is equal to the period of the target orbit $\tau_s = jl\tau_1$.

Motivated by these recent works, we tested both numerically and experimentally the ETDF method with different time-delays on an impact oscillator system described and studied in [27,28]. The current physical model is the same as the one used in [26], and it is depicted in Fig. 1a. It consists of a rigid structure that is mounted on the base. The mass, m, is connected to leaf springs, which are securely clamped between two beams and a grooved base. A permanent cylindrical neodymium magnet is attached to one side of the primary mass using a stainless steel rod and secured by two stainless steel nuts. The magnet is positioned approximately at the centre of a custom-built coil. This setup can provide a direct excitation to the system due to the magnetic coupling. The inner diameter of the coil closely matches the diameter of the cylindrical magnet to enhance the magnetic coupling between the coil and the system, and to minimize nonlinear effects. The coil is powered by a current amplifier, two power suppliers, and a National Instruments board that provides the excitation signal. On either side of the primary mass, there are beams that can be inserted to limit the mass motion by inducing ipacts.

The schematics of the measuring and control system is depicted in Fig. 1, where all signals are collected through a NI-PCI board. An eddy current probe measures the mass displacement, which is then differentiated to obtain velocity. The control signal is calculated by a Labview program and subsequently combined with to the excitation signal. Afterwards, both signals are fed into the coil. The control signal updated frequency is set up as a multiple of the excitation frequency to ensure synchronization and avoid frequency mismatch, and is high enough to justify the assumption of continuous control.

By assuming a linear behaviour of the springs and impact beam, the acceleration X of the mass can be described by Newton's second law:

$$\ddot{X} = -\frac{\kappa_1}{m}X - \frac{c}{m}\dot{X} - \Theta(X-d)\frac{\kappa_2}{m}(X-d) + \frac{F_{coil}}{m}, \tag{3}$$

where d is the gap, Θ is the Heaviside's step function, κ_1 is the primary stiffness, κ_2 is the secondary stiffness, c is an equivalent linear damping coefficient of the system, F_{coil} is the magnetic force applied by the coil and dot represents derivatives in respect to time t.

The coil provides both excitation and actuation to the system. Assuming that a sinusoidal excitation is applied to the system, the system's state $\mathbf{x} = [X, \dot{X}]$ is the observable of the system, the control

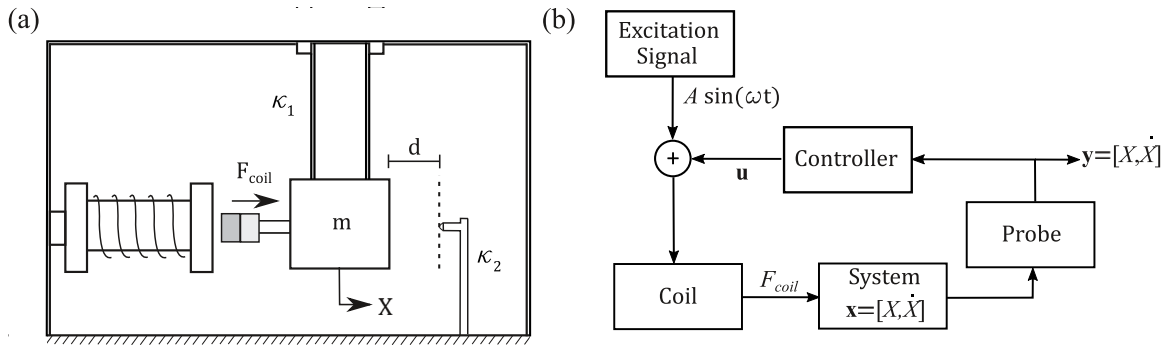

Fig. 1. (a) Schematics of the investigated impact oscillator where, κ_1 is the primary stiffness of the system, κ_2 is the stiffness of the impact beam, d is the gap between the resting position of the oscillator and impact beam, m is the mass, X is the displacement of the oscillator and F_{coil} is the coil force acting on the oscillator. (b) Block diagram of the expermental setup with control.

Table 1
Main parameters of the experimental rig model extracted from [26].

Symbol	Value	Unit	Symbol	Value	Unit
m	1.325	kg	κ_1	4331	N/m
κ_2	87 125	N/m	ω	$2\pi 8.18$	rad/s
d	0.74 10^{-3}	m	A	1.1739	N

is only proportional to velocity, and Eq. (1) is a fast converging series. The coil provides a force given by:

$$F_{coil} = A\sin(\omega t) + k_v\left((1-r)\left(\sum_{n=1}^{10} r^{n-1}\dot{X}(t-n\tau)\right) - \dot{X}(t)\right), \tag{4}$$

where A is the amplitude of excitation, ω is the frequency of excitation and k_v is a proportional gain.

To test and analyse the ETDF, the dynamics of the system should be known. Thus first, we numerically investigate the impact oscillator dynamics without control force **u**. The parameters of the model used are presented in Table 1 as obtained in [26].

Our aim is to identify an UPO that varies its stability characteristics in a wide range of parameters, enabling us to assess ETDF's effectiveness under different scenarios while maintaining the same target. To achieve this, using numerical simulations, we construct bifurcation diagrams for varying damping, c, to identify a wide range of this parameter where an UPO exists. The bifurcation diagram, shown in Fig. 2a, displays the dynamical response of the system and the corresponding values of c chosen for testing the control. A period-1 solution is observed at c ranging from 4.3 kg/s to 10 kg/s. As c decreases below 4.3 kg/s, the period-1 orbit, depicted in Fig. 2g, loses its stability as a period-2 stable orbit emerges, shown in Fig. 2f, through a period-doubling bifurcation. The coexistence persists until $c = 1.8$ kg/s where a strip of chaotic behaviour appears at $c = 0.9$ kg/s. For even lower values of c, windows of chaotic response can be seen up to $c = 0.26$ kg/s. Analysing the diagram, the unstable period-1 orbit, shown in Fig. 2g, becomes a promising candidate to test the controller due to its existence in the wide range of c from 0.2 kg/s to 4.3 kg/s. We further analyse the chaotic response at $c = 0.272$ kg/s, shown in Fig. 2b, to identify the UPOs embedded in its attractor. This is performed by applying the close return method [48] to the Poincaré time series of the system response. Period-1, period-2 and period-5 UPOs, shown respectively in Fig. 2c, Fig. 2d, and Fig. 2e, can be identified.

The damping coefficient of $c = 0.272$ kg/s corresponds to the dissipation from the experimental apparatus [28]. Thus, we choose this value of dissipation to perform our studies and allow comparisons between experimental and numerical results.

Fig. 3 depicts the first performed test to stabilize the target period-1 UPO. Initially, the system has a chaotic response. Subsequently, the control is turned on with a proportional gain of $k_v = 10.8$ kg/s and with a delay equal to one period of the targetted orbit, $\tau = \tau_s = 0.12225$ s, stabilizing the target orbit within a small window of time. After the period-1 is reached, the delay is changed to two periods of the target orbit, $\tau = 2\tau_s = 0.2445$ s. This moves the system away from the period-1 behaviour and stabilizes a period-2 UPO, indicating that the controller cannot maintain the period-1 behaviour with $\tau = 2\tau_s$. Both numerical and experimental results present the same behaviour and have very similar control signals.

A second test is performed and the results are shown in Fig. 4. Initially, the system exhibits a chaotic response and afterwards, the period-1 response is stabilized. When the delay is changed to $\tau = 3\tau_s = 0.36675$ s the period-1 UPO maintains its stability and the system presents no change of behaviour. Finally, we change the control time delay to $\tau = 5\tau_s = 0.61125$ s, which moves the system away from the period-1 orbit originating a chaotic-like behaviour. This indicates that the controller is able to maintain the period-1 UPO stable for $\tau = 3\tau_s$, but is unable to do so for $\tau = 5\tau_s$. As in the previous case, experimental and numerical results are in close agreement with each other.

These two tests do not confirm ETDF's ability to stabilize a periodic response with $\tau = j\tau_s$ delay. In fact, they indicate two main dependencies of the period-1 UPO stability with the time-delay. For even multiples of the period as time delays, $j = 2z$ where z is a positive natural number, the ETDF method is not able to stabilize the period-1 UPO. For odd multiples of the period as time delay, $j = 2z - 1$, the controlled UPO stability is not lost straight away, but it degrades as higher delays are employed. Going forward, we define time delays with odd values of j as odd delays and time delays with even values of j as even delays.

In the following sections, we provide the mathematical basis to analyse this initially counter intuitive dependence of the UPO stability on the control time-delay. To achieve this, we employ the Floquet theory and an equivalence between time-delayed feedback control and proportional control.

3. Analysis of time-delayed feedback methods

The general formulation of a time-delayed control method in a system with state variables **x** and an evolution function **f** can be described by:

$$\dot{\mathbf{x}} = \mathbf{f}(\mathbf{x}, t) + \mathbf{u}(\mathbf{y}(t), \mathbf{y}(t-\tau_1), \mathbf{y}(t-\tau_2)\ldots), \text{ with } \mathbf{y}(t) = \mathbf{C}(\mathbf{x}), \tag{5}$$

where $\mathbf{C}(\mathbf{x})$ is the function describing the observer of the system and τ_i are delays.

Since **u** relies on delayed observations, Eq. (5) becomes a delayed differential equation. Although the application of Lyapunov exponents is very common to assess the stability of an orbit, in the case of delayed systems, it typically involves additional steps and an increased computational effort due to the presence of delays. In comparison to the usual Lyapunov based methods, Floquet theory provides a relation between delayed and current states [49] by evaluating only one period of the

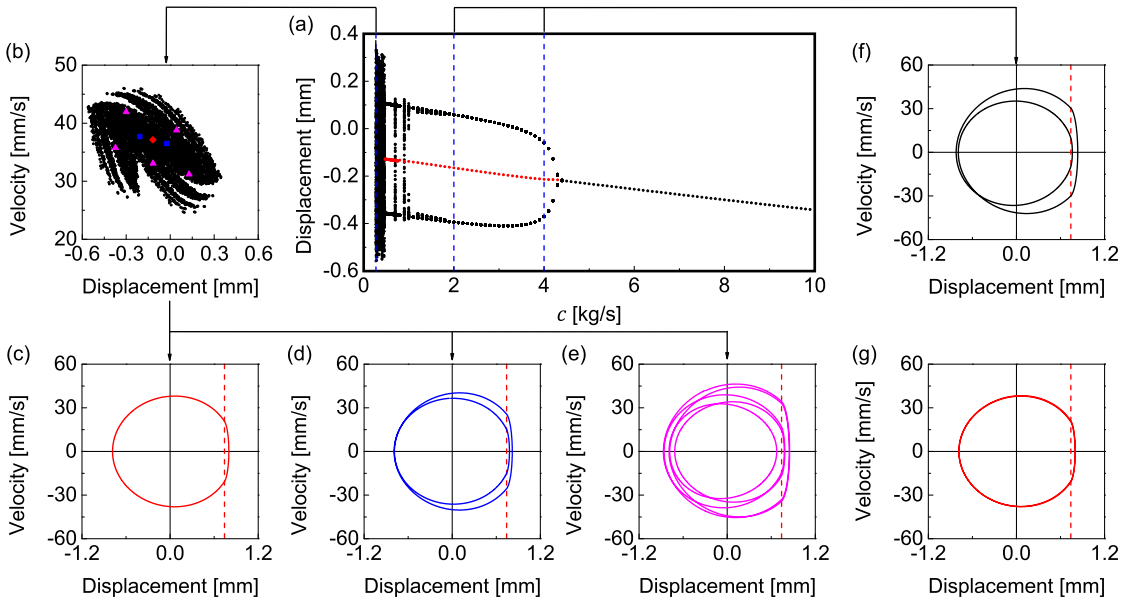

Fig. 2. Dynamic repsonses using c as a bifurcation parameter numerically computed using the parameters in Table 1; (a) numerical bifurcation diagram with varying c; (b) chaotic attractor and Poincaré points of the identified (c) period-1, (d) period-2, and (e) period-5 UPOs at $c = 0.272$ kg/s; (f) trajectory of the stable period-2 orbit on the phase plane at $c = 2$ kg/s; (g) trajectory of the period-1 UPO on the phase plane at $c = 2$ kg/s. Stable attractors are depicted in black while unstable solutions are coloured as period-1 (red), period-2 (blue) and period-5 (magenta). The impact boundary is depicted as a dashed red line on phase planes. (For interpretation of the references to colour in this figure caption, the reader is referred to the web version of this article.).

system response, enabling a more efficient and detailed description of a periodic orbit stability. Thus, we focus our analysis on calculating the Floquet exponents of a controlled orbit.

If a deviation $\boldsymbol{\delta x} = \mathbf{x} - \mathbf{x_0}$ of a periodic orbit $\mathbf{x_0}$ is considered, its evolution is given by:

$$\dot{\boldsymbol{\delta x}} = \nabla_{\mathbf{x}}\mathbf{f}\,\boldsymbol{\delta x}, \tag{6}$$

where $\nabla_{\boldsymbol{x}}$ is the gradient in respect to the $\mathbf{x}$ variable.

As $\nabla_{\mathbf{x}}\mathbf{f}$ is calculated around the orbit $\mathbf{x_0}$ of period τ_s it is also periodic following the equation $\nabla_{\mathbf{x}}\mathbf{f}(t) = \nabla_{\mathbf{x}}\mathbf{f}(t-\tau_s)$. Hence, according to Floquet theory, the solution for Eq. (6) is given by:

$$\boldsymbol{\delta x}(t) = \mathrm{Re}\left(\sum_{i=1}^{N}\left(\boldsymbol{\delta x}(0)\cdot\mathbf{p_i}(0)\right)e^{\mu_i t}\mathbf{p_i}(t)\right), \tag{7}$$

where, N is the dimension of the system, $\mathbf{p_i}(t) = \mathbf{p_i}(t-\tau_s)$ is a periodic function with the same period of the analysed orbit τ_s and μ_i is the Floquet exponent associated with $\mathbf{p_i}$.

Eq. (7) reveals how Floquet exponents are used to analyse the stability of the orbit under consideration. If all real parts of Floquet exponents are lower than zero, $\mathrm{Re}(\mu_i) < 0$, a deviation around the orbit diminishes with time indicating that the orbit is stable. If any of the Floquet exponents has a positive real part, they indicate an unstable orbit.

The most common approach to analyse how the stability of an orbit changes with a parameter, using Floquet exponents, is to plot the real part of the maximum real-valued Floquet exponent, also called the leading Floquet exponent μ_{max}, versus the values of that parameter, as demonstrated in Fig. 5. Whilst considering k as a parameter, the region where $k < k_1$ presents a positive $\mathrm{Re}(\mu_{max})$ indicating an unstable solution, exemplified by Fig. 5b. Hence, the value k_1 is the minimum value of k where the analysed orbit is stable. In the region from $k = k_1$ to $k = k_2$, the orbit is stable since $\mathrm{Re}(\mu_{max}) \leq 0$, shown in Fig. 5c. For values of $k > k_2$, the orbit is unstable, as exemplified in Fig. 5d. Hence, the value k_2 is the maximum value of k where the analysed orbit is stable. Finally, there is an important value of $k = k_{opt}$ where $\mathrm{Re}(\mu_{max})$ reaches its minimum value μ_{opt}.

Whilst at Fig. 5 presents a simple and straightforward way to analyse the stability of an orbit, it overlooks a significant amount of information as it disregards most of the other Floquet exponents and the imaginary part of μ_{max}. A way to obtain a more comprehensive understanding of the full spectrum of Floquet exponents is to track their location in the complex plane as we vary the parameter k, as shown in Fig. 6. In this figure, red crosses represent the values of Floquet exponents at $k = 0$, while black circles represent the values of Floquet exponents at $k \to \infty$. The Floquet exponents evolve from the red crosses to the black circles as k varies, by following the black paths, as depicted by arrows in Fig. 6b. In Fig. 6, the leading Floquet Exponent starts at the rightmost cross and travels left, as k increases, until it crosses to the negative semi-plane, at this point $k = k_1$. Afterwards, the leading Floquet exponent collides with another one on the real axis when $k = k_{opt}$. Subsequently to this collision, the two Floquet exponents move towards the positive semi-plane presenting opposite imaginary parts. Finally, these two exponents cross to the positive semi-plane again at $k = k_2$ and tend to the circles as $k \to \infty$. In this representation, the imaginary part of the Floquet exponents is usually multiplied by the delay of the orbit, τ_s, to compare the shift in phase after a full cycle to multiples of π. This facilitates to identify if a deviation will be in-phase, in anti-phase or de-phased from the analysed orbit.

Following the methods developed by Pyragas et al. [36,41,50] and assuming that $\mathbf{C}$ is linear and has the same dimension as $\mathbf{x}$, the Floquet exponents of an ETDF controlled system can be calculated by obtaining the evolution of $\dot{\boldsymbol{\delta x}}$ as one linearizes Eq. (5) around x_o leading to:

$$\dot{\boldsymbol{\delta x}} = \left(\nabla_{\mathbf{x}}\mathbf{f}(\mathbf{x_0}) + \mathbf{K}\nabla_{\mathbf{x}}\mathbf{C}\nabla_{\boldsymbol{x}}\left((1-r)\left(\sum_{n=1}^{\infty} r^{n-1}\mathbf{x}(t-n\tau)\right) - \mathbf{x}(t)\right)\right)\boldsymbol{\delta x}. \tag{8}$$

By using Eq. (7) one can write the delayed state as:

$$\boldsymbol{\delta x}(t-n\tau) = \mathrm{Re}\left(\sum_{i=1}^{N}\left(\boldsymbol{\delta x}(0)\cdot\mathbf{p_i}(0)\right)e^{\mu_i(t-n\tau)}\mathbf{p_i}(t-n\tau)\right) = e^{-\mathbf{H}_{\boldsymbol{\mu}}n\tau}\boldsymbol{\delta x}(t), \tag{9}$$

and by using the periodicity property of $\mathbf{p_i}(t) = \mathbf{p_i}(t-\tau)$, a relation between the present and delayed states can be obtained as:

$$\boldsymbol{\delta x}(t-n\tau) = \mathrm{Re}\left(\sum_{i=1}^{N} e^{-\mu_i n\tau}\left(\boldsymbol{\delta x}(0)\cdot\mathbf{p_i}(0)\right)e^{\mu_i t}\mathbf{p_i}(t)\right) = e^{-\mathbf{H}_{\boldsymbol{\mu}}n\tau}\boldsymbol{\delta x}(t), \tag{10}$$

where, $\mathbf{H}_{\boldsymbol{\mu}}$ obeys:

$$e^{-\mathbf{H}_{\boldsymbol{\mu}}n\tau} = \mathbf{Q}^{-1}e^{-\mathbf{H}_{\mathbf{diag}}n\tau}\mathbf{Q}, \tag{11}$$

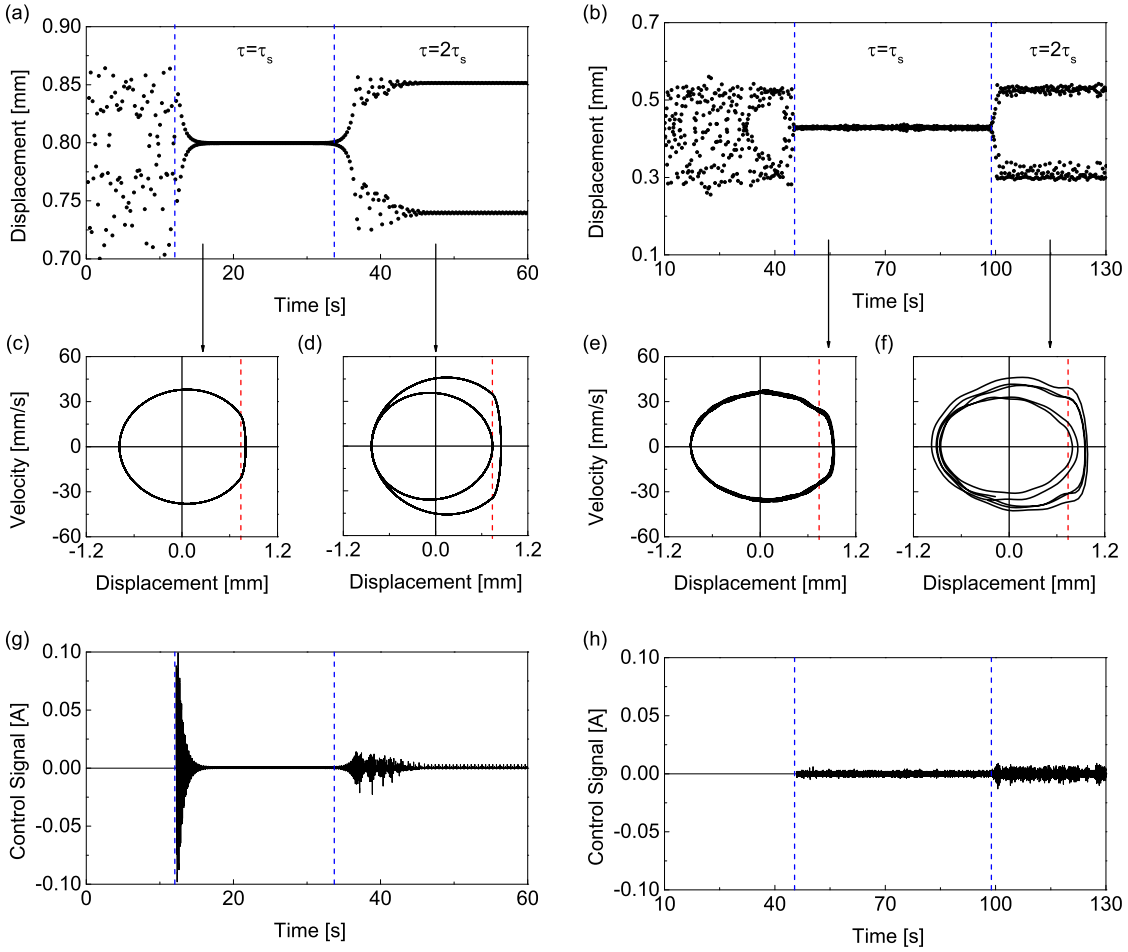

Fig. 3. Numerical and experimental control tests with different delays with a gain $k_v = 10.8$ kg/s and $r = 0$; (a), (b) Poincaré time series of displacement; (c), (e) stabilized target period-1 UPO for $j = 1$; (d), (f) stabilized period-2 UPO for $j = 2$; (g), (h) time history of control current added to the coil. Dashed blue lines indicate when the delay of the control changes and dashed red lines indicate the impact boundary on phase planes. Note that the controller can stabilize the target period-1 UPO only with $j = 1$. (For interpretation of the references to colour in this figure caption, the reader is referred to the web version of this article.).

where, $\mathbf{Q}$ is the transformation for the eigenbase constructed with $\mathbf{p_i}$, and $\mathbf{H_{diag}}$ is a diagonal matrix with the Floquet exponents μ_i as its diagonal elements. Then, by using Eq. (10) the gradient of delayed states can be calculated as:

$$\nabla_{\boldsymbol{x}}\mathbf{x}(t-n\tau) = \nabla_{\delta\mathbf{x}}(\mathbf{x_0}(t)+\delta\mathbf{x}(t-n\tau)) = \nabla_{\delta\mathbf{x}}(\mathbf{x_0}(t)+e^{-\mathbf{H}_{\mu}n\tau}\delta\mathbf{x}(t)) = e^{-\mathbf{H}_{\mu}n\tau}. \tag{12}$$

Substituting this gradient into Eq. (8) and using the formula for a converging infinite sum of a geometric series:

$$\sum_{n=1}^{\infty} r^{n-1}e^{-\mathbf{H}_{\mu}n\tau} = e^{-\mathbf{H}_{\mu}\tau}(\mathbb{I}-re^{-\mathbf{H}_{\mu}\tau})^{-1}, \tag{13}$$

it is obtained:

$$\delta\dot{\mathbf{x}} = \left(\nabla_{\mathbf{x}}\mathbf{f}(\mathbf{x_0}) + \mathbf{K}\nabla_{\mathbf{x}}\mathbf{C}\left(e^{-\mathbf{H}_{\mu}\tau}-\mathbb{I}\right)\left(\mathbb{I}-re^{-\mathbf{H}_{\mu}\tau}\right)^{-1}\right)\cdot\delta\mathbf{x}, \tag{14}$$

where $\mathbb{I}$ is the identity matrix.

After acquiring the evolution of $\delta\mathbf{x}$, one way to calculate the Floquet exponents is to evaluate the fundamental matrix of the system $\boldsymbol{\Psi}$ that is defined as:

$$\delta\mathbf{x}(t) = \boldsymbol{\Psi}(t)\cdot\delta\mathbf{x}(0), \tag{15}$$

where $\boldsymbol{\Psi}(0) = \mathbb{I}$. In sequence, by substituting Eq. (15) into Eq. (14), the evolution of the fundamental matrix is obtained:

$$\dot{\boldsymbol{\Psi}} = \left(\nabla f(\mathbf{x_0}) + \mathbf{K}\nabla_{\mathbf{x}}\mathbf{C}\left(e^{-\mathbf{H}_{\mu}\tau}-\mathbb{I}\right)\left(\mathbb{I}-re^{-\mathbf{H}_{\mu}\tau}\right)^{-1}\right)\boldsymbol{\Psi}. \tag{16}$$

The Floquet exponents are extracted by the diagonalization of the fundamental matrix at τ_s (one period of the analysed orbit). In other words, they are the solution for the equation:

$$(\boldsymbol{\Psi}(\tau_s) - e^{-\mu_i\tau_s}\mathbb{I})\cdot\mathbf{v}_i = \mathbf{0}, \tag{17}$$

where $\mathbf{v}_i$ are the eigenvectors of $\boldsymbol{\Psi}(\tau_s)$.

Several details of Eq. (17) needs to be discussed over as it is transcendental; the function $\boldsymbol{\Psi}(\tau_s)$ depends on the Floquet exponents themselves. Hence, to solve and obtain the Floquet exponents one needs to use an optimization method. Secondly, Eq. (17) has infinitely many solutions on the complex plane, which poses an additional challenge to obtain specific solutions. These difficulties can be minimized if only the stability of the orbit is of concern. In such cases, it is possible to obtain only the leading Floquet exponent, as it dictates stability, and disregard the rest. However, for a full analysis of the control, the remaining FEs cannot be ignored.

Pyragas in [36,41], aiming to circumvent the optimization challenges of Eq. (17), proposed an equivalence between ETDF and proportional gain control. His idea is to assume that an orbit controlled by a proportional gain method has the same Floquet Exponents of an orbit controlled by the ETDF method if the Floquet Exponents are close to the boundary of the first Brillouin zone [41]. To exemplify this equivalence, let us consider the calculation of a deviation $\delta\mathbf{x}$ of an orbit controlled by a proportional gain method with a control signal:

$$\mathbf{u} = \mathbf{G}(\mathbf{y}-\mathbf{y_o}), \tag{18}$$

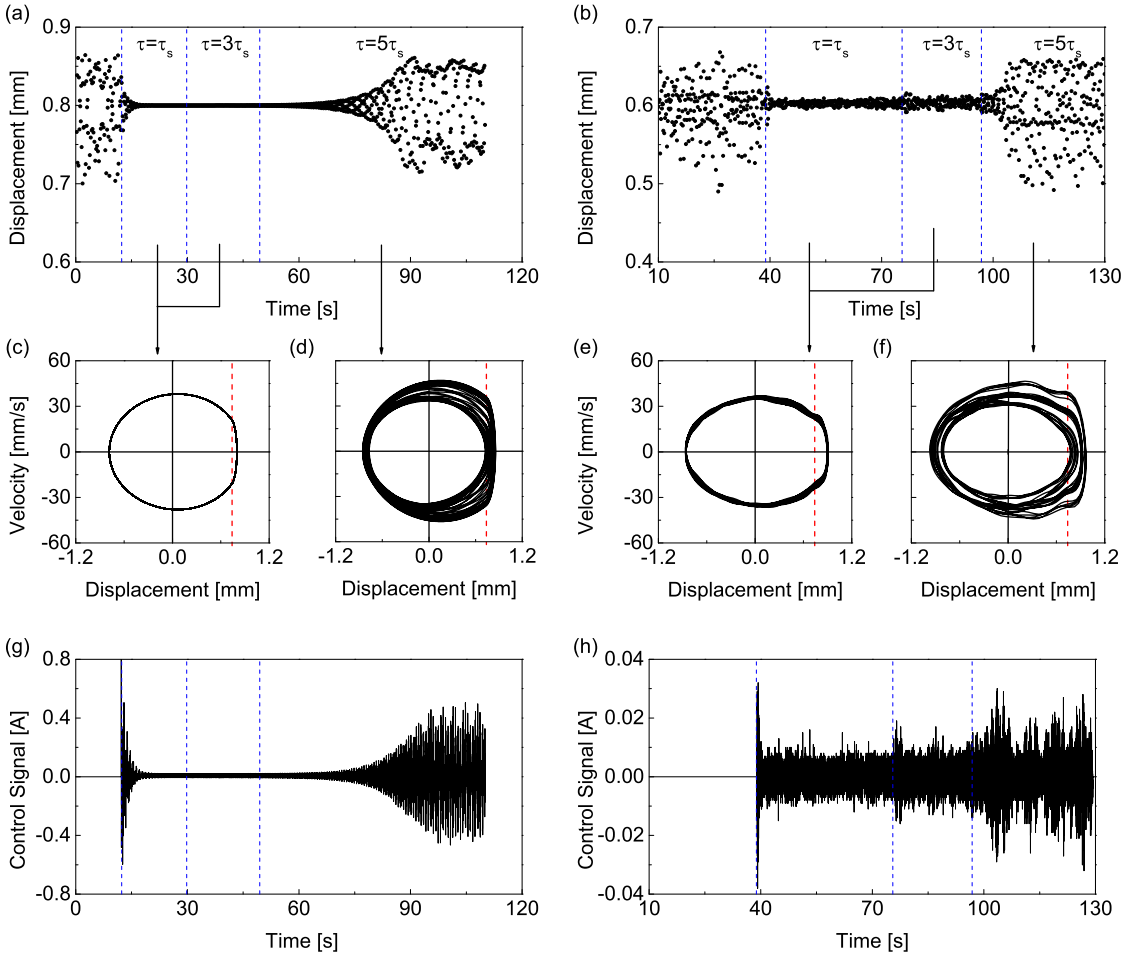

Fig. 4. Numerical and experimental control tests with different delays with a gain k_v = 10.8 kg/s and r = 0; (a), (b) Poincaré time series of displacement. (c), (e) stabilized target period-1 UPO for $j = 1, 3$; (d), (f) system phase plane for $j = 5$; (g), (h) time history of control current added to the coil. Dashed blue lines indicate when the delay of the control changes and dashed red lines indicate the impact boundary on phase planes. Note that the controller can stabilize the target period-1 UPO only with $j = 1$ and $j = 3$. (For interpretation of the references to colour in this figure caption, the reader is referred to the web version of this article.).

where $\mathbf{G}$ is the proportional gain matrix.

In this case, the evolution of the deviation is given by:

$$\delta\dot{\mathbf{x}} = \left(\nabla_{\mathbf{x}}\mathbf{f}(\mathbf{x_0}) - \mathbf{G}\nabla_{\mathbf{x}}\mathbf{C}\right)\delta\mathbf{x}. \tag{19}$$

Thus, the fundamental matrix evolution equation can have the following form:

$$\dot{\mathbf{\Psi}} = \left(\nabla_{\mathbf{x}}\mathbf{f}(\mathbf{x_0}) - \mathbf{G}\nabla_{\mathbf{x}}\mathbf{C}\right)\mathbf{\Psi}. \tag{20}$$

By using Eq. (20), the Floquet Exponents of the controlled orbit can than be presented as a function of the proportional gains $s_i(\mathbf{G})$. Accordingly, in the following discussion, we denote the Floquet exponents related to proportional gain control as s_i, while those associated with ETDF control are denoted as μ_i.

If Eqs. (16) and (20) are compared, their only difference is that the second term of the former is real while in the latter it can be complex. Hence, if it is assumed that the terms in both equations are real, in other words:

$$\Im\left(\mathbf{K}\nabla_{\mathbf{x}}\mathbf{C}\left(e^{-\mathbf{H}_{\mu}\tau} - \mathbb{I}\right)\left(\mathbb{I} - re^{-\mathbf{H}_{\mu}\tau}\right)^{-1}\right) = \mathbf{0}, \tag{21}$$

where $\Im$ is an operator that extracts the imaginary part of a complex number. Then, both equations are equivalent and the Floquet Exponent of the orbit controlled by the proportional gain will be the same for the orbit controlled by the ETDF, $s_i(\mathbf{G}) = \mu_i$. As such, one can equalize the second term Eqs. (16) and (20) establishing a relation between the ETDF gains $\mathbf{K}$ that result in the same FE of a given proportional gain $\mathbf{G}$.

$$\mathbf{K}\nabla_{\mathbf{x}}\mathbf{C}\left(e^{-\mathbf{H}_{\mu}\tau} - \mathbb{I}\right)\left(\mathbb{I} - re^{-\mathbf{H}_{\mu}\tau}\right)^{-1} = -\mathbf{G}\nabla_{\mathbf{x}}\mathbf{C}. \tag{22}$$

As the Floquet exponents can be assumed to be the same, we replace $\mathbf{H}_{\mu}$ with the matrix $\mathbf{H}_{\mathbf{s}}$ that is related to the Floquet Exponents of the given proportional gains $s_i(\mathbf{G})$. Then, by rearranging the equation one obtains,

$$\mathbf{K} = -\mathbf{G}\nabla_{\mathbf{x}}\mathbf{C}\left(\mathbb{I} - re^{-\mathbf{H}_{\mathbf{s}}\tau}\right)\left(e^{-\mathbf{H}_{\mathbf{s}}\tau} - \mathbb{I}\right)^{-1}\left(\nabla_{\mathbf{x}}\mathbf{C}\right)^{-1}. \tag{23}$$

Eq. (23) can then be used to relate the Floquet exponents, r and the ETDF gain. To illustrate this, let us assume that the observations are performed directly into one state, so $\mathbf{C}$ can be considered as a scalar $C = x_i$, and that feedback is only performed on one state variable so that $\mathbf{K}$ and $\mathbf{G}$ become a scalar k and g, respectively.

If we also assume that delay is a multiple of the target orbit period, $\tau = j\tau_s$, Eq. (23) can be rewritten as:

$$k = -g\left(1 - re^{-s_i(g)j\tau_s}\right)\left(e^{-s_i(g)j\tau_s} - 1\right)^{-1}. \tag{24}$$

As Eq. (24) is assumed to yield a real value, the Floquet Exponents can be written as:

$$s_i(g)\tau_s = s_{ri}(g)\tau_s + i\pi, \tag{25}$$

where s_{ri} is the real part of s_i. If a linear dependence is assumed for $s_{ri}(g)$:

$$s_{ri}(g) = \mu_0(1 - g/g_1), \tag{26}$$

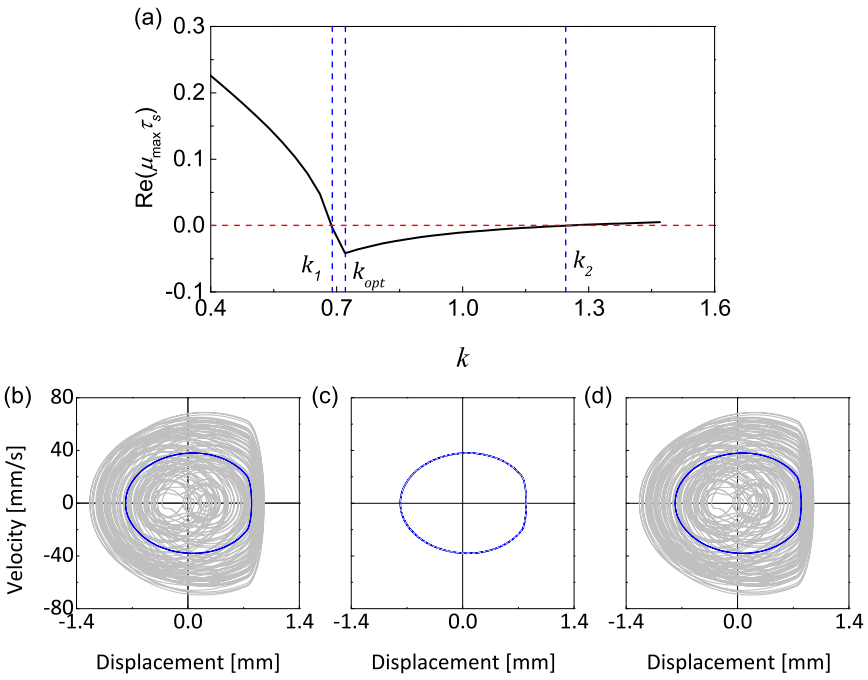

Fig. 5. Evaluation of the periodic orbit stability; (a) real part of the maximum real valued Floquet exponent, with the limit of stability depicted by a dashed red line. Phase planes examples depicting the considered periodic orbit (blue) and obtained response (light grey) with different values of k; (b) divergence of the analysed orbit for lower values $k < k_1$; (c) convergence to the orbit for $k \in [k_1, k_2]$; (d) divergence of the analysed orbit for higher values $k > k_2$. (For interpretation of the references to colour in this figure caption, the reader is referred to the web version of this article.).

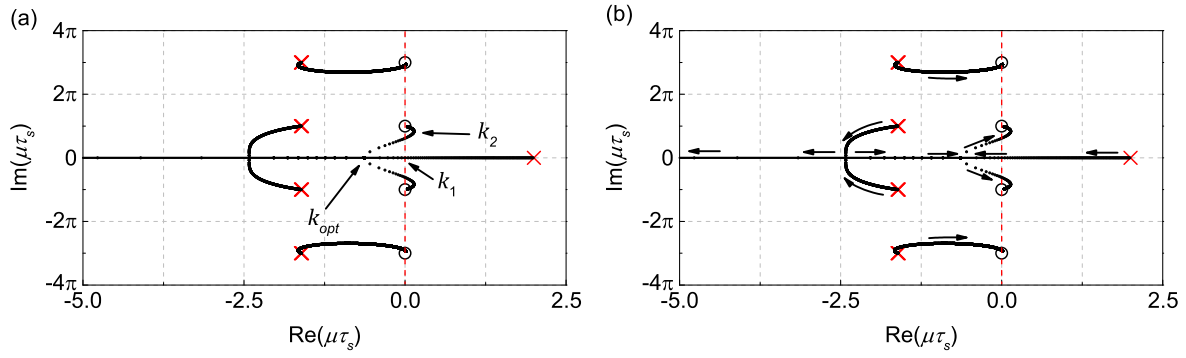

Fig. 6. Example analysis of ETDF using Floquet theory; (a) Floquet exponents in the complex plane and their path as a parameter k is varied; (b) path directions of Floquet exponents in the complex plane highlighted by arrows. The exponents migrate from the red crosses were $k = 0$, (×) to the circles as $k \to \infty$, (○).

leading to:

$$g = \frac{g_1}{\mu_0}(\mu_0 - s_{ri}(g)), \tag{27}$$

where μ_0 is the orbit Floquet Exponent real part without control, also referenced as the original instability of the orbit, and g_1 is the critical gain where the orbit becomes stable. Subsequently, the relation between the ETDF gain and Floquet Exponents can be obtained by substituting Eqs. (25) and (27) into (24),

$$k = \frac{g_1}{\mu_0}(\mu_0 - s_{ri})\frac{1 + r(-1)^{j+1}e^{-s_{ri}j\tau_s}}{(-1)^{j+1}e^{-s_{ri}j\tau_s} + 1}. \tag{28}$$

Finally, by solving Eq. (28) for a given k, the controlled orbit full spectrum of Floquet exponents can be obtained. It is also highlighted that the term $\frac{g_1}{\mu_0}(\mu_0 - s_{ri})$ of Eq. (28) gives the Floquet exponent related to the system itself as it contains the orbits Floquet Exponent without control μ_0 and the critical gain g_1. Whilst the rest of the equation generates the Floquet Exponents related to the control and the introduction of delayed states.

Eq. (28) can also be used to predict some features of ETDF. For the sake of simplicity, let us analyse the system on the first boundary of stability, such as $s_{ri} = 0$. In this case, the first critical gain k_1 for ETDF can be calculated by:

$$\frac{k_1}{g_1} = \frac{1 + r(-1)^{j+1}}{(-1)^{j+1} + 1}. \tag{29}$$

Note that the Eq. (29) has only a solution when $j = 2n - 1$, $n \in \mathbb{N}$. This already indicates that a critical gain only exists for odd multiples of the time-delay. It also implies that the critical gain k_1 is unaffected by changes in odd delays. Finally, it also shows that ETDF's critical gain k_1 is directly proportional to the proportional feedback critical gain g_1 by a factor $0.5+r/2$. This indicates that increases in r increase the value of critical gain k_1.

Having established the mathematical framework of our analysis, we proceed to the next session, where we conduct a parametric investigation of ETDF by calculating the full spectrum of Floquet exponents of the controlled period-1 orbit of the impact oscillator system.

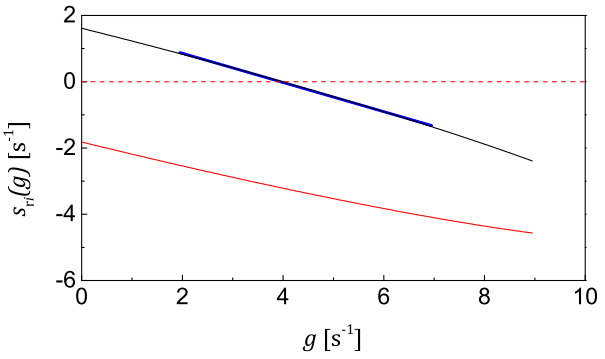

Fig. 7. Floquet exponents of the period-1 orbit with proportional gain. The leading FE is depicted in black and minimum in red. A linear approximation of the leading FE dependency is given in blue. (For interpretation of the references to colour in this figure caption, the reader is referred to the web version of this article.).

4. Parametric analysis of ETDF applied to the impact oscillator

In this section, we analyse the period-1 UPO of the impact oscillator and aim to provide an explanation for the results presented in Section 2 by utilizing the mathematical methods introduced previously.

The first task performed was to obtain the function $s_{ri}(g)$ for the orbit controlled by a proportional control by directly solving Eq. (20). This is done by assuming a control signal given by:

$$\mathbf{u} = \begin{bmatrix} 0 \\ u \end{bmatrix} = \begin{bmatrix} 0 \\ g(\dot{x}_o - \dot{x}) \end{bmatrix}. \tag{30}$$

The results presented in Fig. 7 demonstrate a linear relationship between the leading Floquet exponent (black line) and the proportional gain g. This confirms the previous assumptions made in Eq. (27). Thus, by fitting a linear approximation near zero (blue line), we can obtain the initial leading Floquet exponent real part $\mu_0 = 1.73876\ s^{-1}$ and the critical gain $g_1 = 3.94\ s^{-1}$. Furthermore, the secondary Floquet exponent, shown in red, also presents a linear behaviour for small g.

4.1. Influence of different delays

With the identified parameters, we can utilize Eq. (28) to examine the paths of the Floquet exponent in the complex plane as the proportional gain in the impact oscillator control k_v is varied. Fig. 8 shows these paths for the delays used in Section 2 and $r = 0$. It is important to highlight that the crosses located in the negative semi-plane are not shown in the figure. This is because, when $r = 0$, the real part of Floquet exponents related to the control tends to $-\infty$. Also, as a delayed system has an infinite number of Floquet exponents, only the four (five) Floquet exponents with the smallest imaginary parts are displayed in the figure.

Analysing the variations due to delay, Figs. 8a, 8c and 8d show that, for odd multiples of the delay, the Floquet exponents collide with each other on the real axis defining μ_{opt}. Afterwards, the colliding leading Floquet exponents become complex conjugates and migrate towards the circles at the imaginary axis. Analysing the effect of altering odd delays, the figures show that higher values of delay bring the circles in the imaginary axis closer together, which brings the Floquet exponents collision closer to the positive semi-plane. As a consequence, the value of μ_{opt} increases and the value of k_2 decreases as the Floquet exponents paths start crossing to the positive semi-plane before reaching the black circles. The same does not happen for even multiples of delay, as the path's structures change completely from their odd counterpart. Fig. 8b shows that even multiples of delay shift the circles along the complex axis creating a blockade in the imaginary axis. A circle, shifted to the origin of the graph, does not allow the leading Floquet exponent to cross to the negative semi-plane eliminating the control's ability to stabilize the orbit. Furthermore, multiples of even delay have the effect of bringing the circles on the imaginary axis close together in the same way as seen for odd delays, however, they all present a circle at the origin which does not allow the leading Floquet exponent to migrate to the negative semi-plane.

We validate our calculations by comparing the predicted $\mathrm{Re}(\mu_{max})$ with k_v by Eq. (28) with the values obtained by solving numerically Eqs. (16) and (17). An optimization algorithm presented in [28] is used to solve the full set of these equations. Fig. 9 shows a comparison of both results for various values of delay. As expected, only odd multiples of delay present negative values of μ_{max} while for $\tau = 2\tau_s$ there were no values of k_v that could control the orbit. Also, both odd delay curves become negative at the same value of k_v, showing that k_1 does not change with the increase in delay as predicted by Eq. (29).

When comparing both calculations (dashed–dotted and solid lines), we observe a close agreement between them. Only a small difference can be seen when the Floquet exponents reach μ_{opt}, however, this difference diminishes as k_v increases. This is also consistent with our assumptions. The Floquet exponents near μ_{opt} deviate from the real axis making our assumption that $\Im\mu_i = n\pi$ invalid, which produces the maximum absolute difference between the methods, shown in Fig. 9b. Subsequently, as k_v increases the Floquet exponents come closer to our assumption $\Im\mu_i = n\pi$ which reduces the approximation error.

Finally, if the value of $k_v = 10.8$ kg/s is considered (dashed vertical blue line) an agreement with the results in Section 2 can be obtained. Fig. 9 shows that the only multiple delays that can stabilize the orbit for this gain is $\tau = 3\tau_s$, while $\tau = 2\tau_s$ and $\tau = 5\tau_s$ have a positive μ_{max} indicating that the orbit would be unstable. This perfectly agrees with the experimental and numerical results obtained previously.

We further investigate the influence of odd delays on the Floquet exponents for $r = 0.1$ to see how it can affect their values for $k_v \approx 0$ (red crosses). When $r \neq 0$, crosses on the negative semi-plane assume finite values, as shown in Fig. 10. There are two collisions of Floquet exponents located on the real axis. The first collision, happening at a lower real value, involves Floquet exponents related to the ETDF control. The second collision, at a higher real value, involves the leading Floquet exponent and another related to the control and defines μ_{opt}. If we compare both panels, the effect of changing the delay brings the crosses and circles together and pushes the second collision to the positive semi-plane making the orbit uncontrollable in this scenario. Thus, changing the delays not only changed the imaginary part of crosses but also their real value, bringing them closer to the positive semi-plane. Finally, we can conclude that raising the value of r increases the influence of odd delays on the Floquet exponents.

In summary, **a ETDF control that has even multiples of an orbit as delay cannot stabilize this orbit**. This proves that there is no risk of inadvertently stabilizing, for example, a period-1 UPO while targetting a period-2 UPO and explains also previous results obtained for other systems [51]. However, although there is deterioration of stability, it is possible to stabilize an orbit when using odd delays, for instance, stabilizing a period-1 UPO while targetting a period-3 UPO.

4.2. Effect of original instability

In addition to the influence of delays, the methods presented can also be used to analyse the effect of the original instability μ_0 on the control effectiveness. This is accomplished by analysing an unstable period-1 orbit existing in the range of damping coefficient depicted in Fig. 2. More specifically, we choose the values of $c = 10^{-6}, 2,$ and 4 kg/s corresponding to the initial instabilities values of $\mu_0 = 1.833, 1.002, 0.138\ s^{-1}$, respectively. We follow the same procedure as in Fig. 7 to obtain g_1 and μ_0 for these values of c and consequently solve Eq. (28).

Fig. 11 shows the paths of the Floquet exponents in the complex plane for the three aforementioned cases. For this analysis, it is useful to consider crosses as sources and circles as sinks. In Fig. 11a, the red

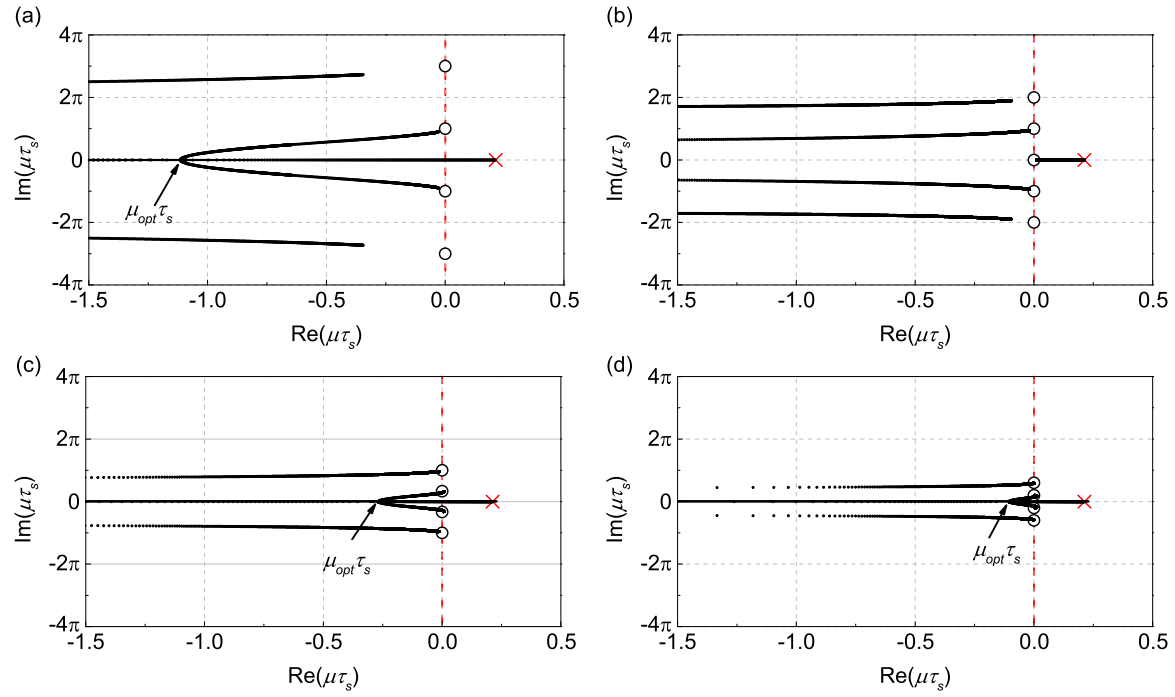

Fig. 8. Floquet exponents paths in the complex plane for the period-1 UPO, $r = 0$; (a) $j = 1$; (b) even delay $j = 2$; (c) $j = 3$ and (d) $j = 5$. Red crosses (×) indicate when $k = 0$ and black circles (○) indicates when $k \to \infty$. Note that because $r = 0$ the crosses related to the control are at $\mathrm{Re}(\mu) = \infty$ s^{-1} and not depicted in the figure. Some paths in (a) and (b) do not reach the circles as calculations were made up to a maximum value of $k_v = k_{lim}$.

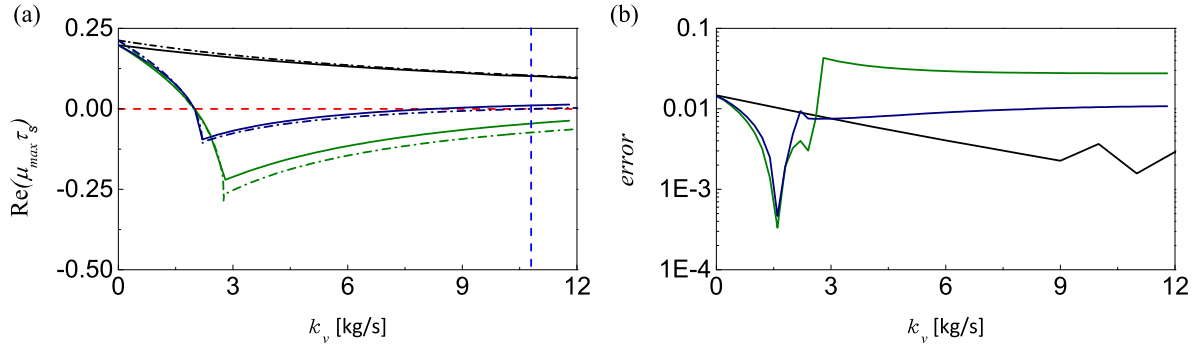

Fig. 9. (a) Comparison between the leading Floquet exponents of the period-1 UPO calculated by the proportional gain approximation (dashed dotted lines) and by original transcendental Eqs. (16) and (17) (solid lines) for several values of delay: $j = 2$ in black, $j = 3$ in green, and $j = 5$ in navy. The experiment gain value is highlighted with a vertical dashed blue line; (b) absolute difference between both methods. Note that the maximum absolute difference occurs when $Re(\mu_{max})$ is minimum. (For interpretation of the references to colour in this figure caption, the reader is referred to the web version of this article.).

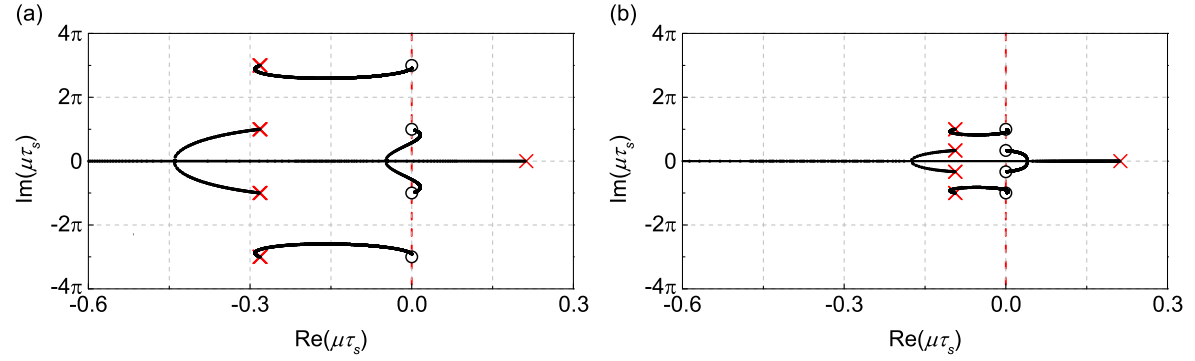

Fig. 10. Floquet exponents paths in the complex plane for the period-1 UPO, $r = 0.1$; (a) $j = 1$ stabilization of the target orbit is achieved with appropriate value of k_v; (b) $j = 3$ stabilization of the target orbit cannot be achieved for all values of k_v. Note that the increase in r makes the orbit unstable for $j = 3$. Red crosses (×) indicate when $k = 0$ and black circles (○) indicates when $k \to \infty$.

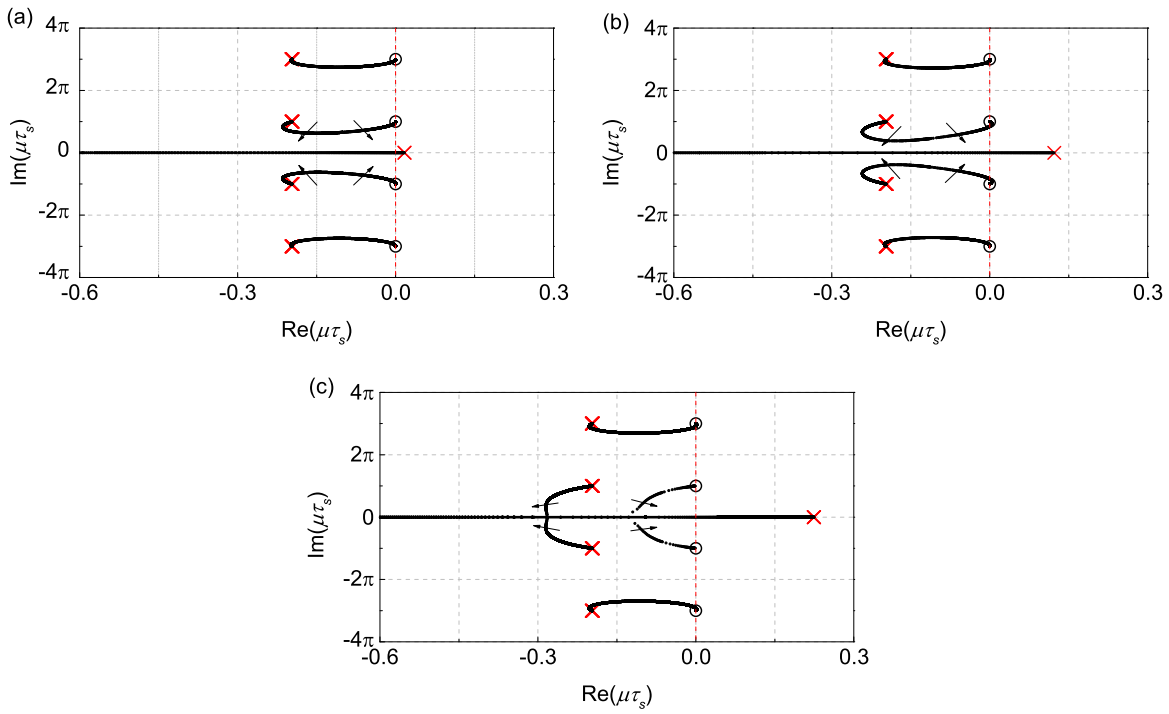

Fig. 11. Floquet exponents paths in the complex plane for the period-1 UPO, $r = 0.2$ and several values of μ_0. The initial instability of the orbit is changed by adjusting the damping coefficient in the existence range of the UPO from $c = 10^{-6}$ kg/s to $c = 4$ kg/s as depicted in Fig. 2; (a) $c = 4$ kg/s, $\mu_0 = 0.138$ s^{-1}; (b) $c = 2$ kg/s, $\mu_0 = 1.002$ s^{-1}; (c) $c = 10^{-6}$ kg/s, $\mu_0 = 1.833$ s^{-1}. Red crosses (×) indicate when $k = 0$ and black circles (○) indicates when $k \to \infty$. Arrows indicate the movement of the Floquet exponent paths as the initial instability increases.

cross located on the positive semi-plane corresponding to the Floquet exponent related to the system, repels the other Floquet exponents from the real axis. As μ_0 increases, Fig. 11b, the cross moves further away, letting the paths on each side of the real axis to approach one another. Further increases in μ_0, make the paths on each side of the real axis merge with the path on the real axis creating two collisions of Floquet exponents, as seen in Fig. 11c.

Due to the relatively narrow range of μ_0 in which identified period-1 UPOs are present, all the phenomena in Eq. (28) cannot be verified. To provide a more comprehensive analysis of the presented method, we consider values of μ_0 unrelated to the impact oscillator system. Fig. 12 shows the Floquet exponents paths in the complex plane for a broader range of initial instabilities. It depicts the same behaviour described previously in Fig. 11 until the final panel, where the initial instability is sufficiently high to move the collision defining μ_{opt} to the positive semi-plane. This indicates that the ETDF method is not be able to control the orbit regardless of the gains, which puts a limit on initial instability for the orbit to be effectively controlled.

We also analyse the effects of μ_0 in the dependence of μ_{max} on k in Fig. 13. As μ_0 increases it shifts the curves to the right and upwards while flattening variations of the Floquet exponents after the minimum value of the curves, μ_{opt}. With these observations in mind, we extract the values of k_1 and k_{opt} from the curves and graph them against the values of μ_0 in Fig. 13b. Notably, we observe that there is a linear dependence of k_1 with μ_0 which enables us to predict the maximum initial instability for the ETDF method to be effective, μ_0^*. This is performed by calculating the value of μ_0 at the crossing between the values of k_{opt} and the line defining the values of k_1.

In summary, a linear dependence of the initial gain k_1 with the original instability of an orbit μ_0 can be confirmed and used to predict the maximum μ_0 of an orbit that the ETDF method can be effective. This valuable insight enables to design a ETDF controller with fewer calculations of Floquet exponents and also to facilitate an evaluation of the ETDF's robustness to orbit instabilities due to variations in the system parameters.

5. Conclusions

In this study, we provided insights into applications of the ETDF with delays that are multiples of the targetted orbit's period and its effects on the Floquet exponents of a controlled orbit. In particular, this was done for the counter-intuitive ETDF's inability to stabilize its target orbit when using a delay that is even multiple of the targetted orbit's period. Specifically, we characterize the dynamics of an impact oscillator and perform the numerical and experimental control of an identified period-1 UPO. After performing the tests, we observed an unexpected loss of ETDF's effectiveness when using that are even multiples or high odd multiples of the orbit's period. To further analyse this phenomenon, we present a methodology to calculate an ETDF controlled orbit Floquet exponents by utilizing an equivalence between ETDF and proportional control. Furthermore, we validated these assumptions for a non-smooth dynamical system.

Additionally, we conducted a comprehensive parametric analysis of different delays. Our findings reveal that ETDF fails to stabilize an orbit using even multiples of its delay due to the shift in the imaginary part of Floquet exponents when $k \to \infty$. Moreover, we analysed odd multiples of delay and discover that increases in the multiplicity of the delay deteriorate the controlled orbit stability up to a critical point at which ETDF loses its ability to successfully stabilize the orbit. Furthermore, we explored the influence of the orbit's initial instability on the efficacy of ETDF, and then proposed a simple method to predict the maximum instability in which ETDF becomes ineffective in stabilizing the orbit.

The analysis conducted in this work provides insights into the underlying phenomena of time-delayed methods and lays foundations for further developments of time-delayed control methods. It also provide a mathematical basis for the analysis of the ETDF with different time-delays which can help control designs for nonlinear systems.

Declaration of competing interest

The authors declare that they have no known competing financial interests or personal relationships that could have appeared to influence the work reported in this paper.

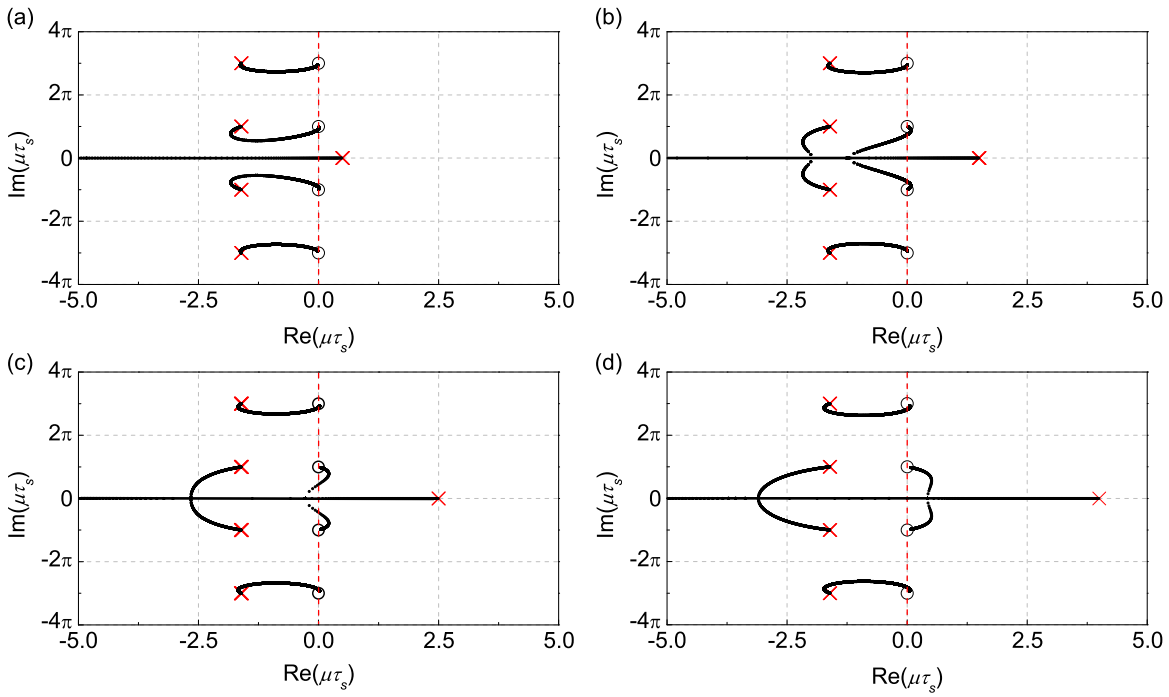

Fig. 12. Initial orbit instability effect on Floquet exponents for $r = 0.2$ and $\tau_s = 1$ s; (a) $\mu_0 = 0.5$ s^{-1} the exponents paths do not collide; (b) $\mu_0 = 1.5$ s^{-1} is high enough to allow paths to collide; (c) $\mu_0 = 2.5$ s^{-1} the point where collision happens gets pulled to the right as initial instability increases; (d) $\mu_0 = 4$ s^{-1} Floquet exponents paths collide with each other on the positive semi-plane indicating that there is no value of k that can stabilize the orbit. Red crosses (×) indicate when $k = 0$ and black circles (○) indicates when $k \to \infty$.

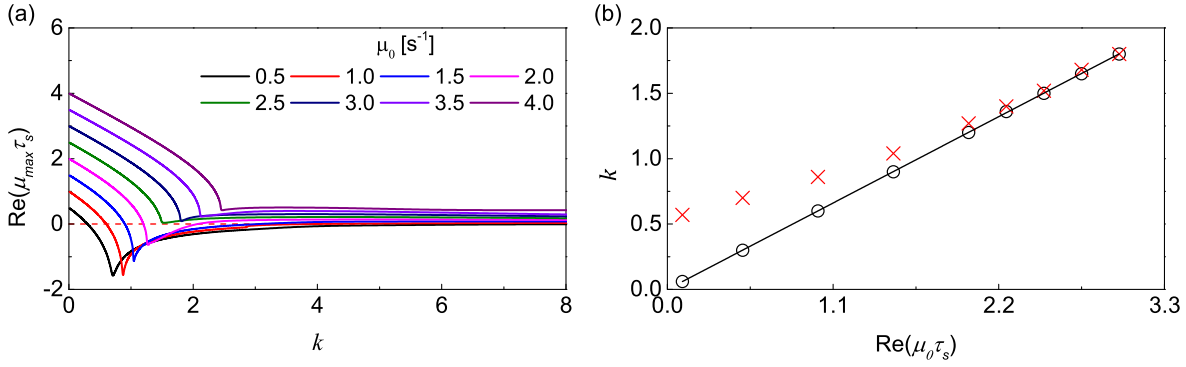

Fig. 13. Prediction of the maximum controllable instability μ_0^*; (a) analysis of μ_{max} dependence of k for several initial instabilities μ_0 and $r = 0.2$; (b) values of k_1, black circles (○) and k_{opt} (×) for several values of μ_0. The black line indicates a linear fit of the dependence of k_1 with initial instability μ_0.

Data availability

Data will be made available on request.

References

[1] Pyragas K. Continuous control of chaos by self-controlling feedback. Phys Lett A 1992;170:421–8.
[2] De Paula AS, Savi MA, Vaziri V, Pavlovskaia E, Wiercigroch M. Experimental bifurcation control of a parametric pendulum. J Vib Control 2017;23(14):2256–68.
[3] Ding Y, Zheng L, Yang R. Time-delayed feedback control of improved friction-induced model: application to moving belt of particle supply device. Nonlinear Dynam 2020;100(1):423–34.
[4] Kirrou I, Belhaq M. Control of bistability in non-contact mode atomic force microscopy using modulated time delay. Nonlinear Dynam 2015;81(1):607–19.
[5] Tusset AM, Ribeiro MA, Lenz WB, Rocha RT, Balthazar JM. Time delayed feedback control applied in an atomic force microscopy (AFM) model in fractional-order. J Vib Eng Technol 2020;8(2):327–35.
[6] Paul B, Banerjee T. Nonlocal time-delayed feedback control of spatiotemporal patterns: controlling a network of digital phase-locked loops. Nonlinear Dynam 2019;96(2):811–23.
[7] Schikora S, Wünsche HJ, Henneberger F. All-optical noninvasive chaos control of a semiconductor laser. Phys Rev E 2008;78(2):025202.
[8] Ferreira BB, Savi MA, De Paula AS. Chaos control applied to cardiac rhythms represented by ECG signals. Phys Scr 2014;89(10):105203.
[9] Watanabe M, Sakai K. Delayed feedback control for chaotic vibration in nonlinear impact dynamics of bouncing agricultural tractor. Sci Rep 2023;13(1):10695.
[10] Pyragas K, Tamasevicius A. Experimental control of chaos by delayed self-controlling feedback. Phys Lett A 1993;180(2):99–102.
[11] Socolar JES, Sukow DW, Gauthier DJ. Stabilizing unstable periodic orbits in fast dynamical systems. Phys Rev E 1994;50(4):3245–8.
[12] Lehnert J, Hövel P, Flunkert V, Guzenko PY, Fradkov AL, Schöll E. Adaptive tuning of feedback gain in time-delayed feedback control. Chaos 2011;21(4):043111.
[13] Selivanov A, Lehnert J, Fradkov A, Schöll E. Adaptive time-delayed stabilization of steady states and periodic orbits. Phys Rev E 2015;91(1):012906.
[14] Pyragas V, Pyragas K. Adaptive modification of the delayed feedback control algorithm with a continuously varying time delay. Phys Lett A 2011;375(44):3866–71.
[15] Pyragas K. Control of chaos via an unstable delayed feedback controller. Phys Rev Lett 2001;86(11):2265–8.
[16] Ushio T. Limitation of delayed feedback control in nonlinear discrete-time systems. IEEE Trans Circuits Syst I 1996;43(9):815–6.
[17] Stépán G, Insperger T. Stability of time-periodic and delayed systems — A route to act-and-wait control. Annu Rev Control 2006;30(2):159–68.

[18] Leonov GA. Pyragas stabilizability via delayed feedback with periodic control gain. Systems Control Lett 2014;69:34–7.
[19] Pyragas V, Pyragas K. Act-and-wait time-delayed feedback control of nonautonomous systems. Phys Rev E 2016;94(1):012201.
[20] Pyragas V, Pyragas K. Act-and-wait time-delayed feedback control of autonomous systems. Phys Lett A 2018;382(8):574–80.
[21] Pyragas V, Pyragas K. State-dependent act-and-wait time-delayed feedback control algorithm. Commun Nonlinear Sci Numer Simul 2019;73:338–50.
[22] De Paula AS, Savi MA, Wiercigroch M, Pavlovskaia E. Bifurcation control of a parametric pendulum. Int J Bifurcation Chaos 2012;22(5):1250111.
[23] Costa DDA, Savi MA, De Paula AS, Bernardini D. Chaos control of a shape memory alloy structure using thermal constrained actuation. Int J Non-Linear Mech 2019;111:106–18.
[24] Voss HU. Anticipating chaotic synchronization. Phys Rev E 2000;61(5):5115–9.
[25] Voss HU. Dynamic long-term anticipation of chaotic states. Phys Rev Lett 2001;87(1):014102.
[26] Costa DDA, Vaziri V, Pavlovskaia E, Savi MA, Wiercigroch M. Switching between periodic orbits in impact oscillator by time-delayed feedback methods. Physica D 2023;443:133587.
[27] Wiercigroch M, Kovacs S, Zong S, Costa D, Vaziri V, Kapitaniak M, et al. Versatile mass excited impact oscillator. Nonlinear Dynam 2020;99(1):323–39.
[28] Costa DDA, Vaziri V, Kapitaniak M, Kovacs S, Pavlovskaia E, Savi MA, Wiercigroch M. Chaos in impact oscillators not in vain: dynamics of new mass excited oscillator. Nonlinear Dynam 2020;102(2):835–61.
[29] Zhang Z, Chávez JP, Sieber J, Liu Y. Controlling grazing-induced multistability in a piecewise-smooth impacting system via the time-delayed feedback control. Nonlinear Dynam 2021;107:1595–610.
[30] Zhang Z, Chávez JP, Sieber J, Liu Y. Numerical analysis of a multistable capsule system under the delayed feedback control with a constant delay. Int J Non-Linear Mech 2023;152:104390.
[31] De Paula AS, Savi MA. Controlling chaos in a nonlinear pendulum using an extended time-delayed feedback control method. Chaos Solitons Fractals 2009;42(5):2981–8.
[32] Nakajima H, Ueda Y. Half-period delayed feedback control for dynamical systems with symmetries. Phys Rev E 1998;58(2):1757.
[33] Fiedler B, Flunkert V, Georgi M, Hövel P, Schöll E. Refuting the odd-number limitation of time-delayed feedback control. Phys Rev Lett 2007;98(11):114101.
[34] Chen G, Yu X. On time-delayed feedback control of chaotic systems. IEEE Trans Circuits Syst I 1999;46(6):767–72.
[35] Just W, Bernard T, Ostheimer M, Reibold E, Benner H. Mechanism of time-delayed feedback control. Phys Rev Lett 1997;79(2):203–6.
[36] Pyragas K. Analytical properties and optimization of time-delayed feedback control. Phys Rev E 2002;66(2):026207.
[37] Brandstetter S, Dahlem MA, Schöll E. Interplay of time-delayed feedback control and temporally correlated noise in excitable systems. Phil Trans R Soc A 2010;368(1911):391–421.
[38] Sieber J. Generic stabilizability for time-delayed feedback control. Proc R Soc A: Math, Phys Eng Sci 2016;472(2189):20150593.
[39] von Loewenich C, Benner H, Just W. Experimental relevance of global properties of time-delayed feedback control. Phys Rev Lett 2004;93(17):174101.
[40] Höhne K, Shirahama H, Choe C, Benner H, Pyragas K, Just W. Global properties in an experimental realization of time-delayed feedback control with an unstable control loop. Phys Rev Lett 2007;98(21):214102.
[41] Pyragas K. Delayed feedback control of chaos. Phil Trans R Soc A 2006;364(1846):2309–34.
[42] Ikeda K, Matsumoto K. High-dimensional chaotic behavior in systems with time-delayed feedback. Physica D 1987;29(1):223–35.
[43] Purewall AS, Postlethwaite CM, Krauskopf B. Effect of delay mismatch in pyragas feedback control. Phys Rev E 2014;90(5):052905.
[44] Friart G, Verschaffelt G, Danckaert J, Erneux Thomas. All-optical controlled switching between time-periodic square waves in diode lasers with delayed feedback. Opt Lett 2014;39:6098–101.
[45] Balanov AG, Janson NB, Schöll E. Delayed feedback control of chaos: Bifurcation analysis. Phys Rev E - Stat, Nonlinear, Soft Matter Phys 2005;71(1):016222.
[46] Hizanidis J, Aust R, Schöll E. Delay-induced multistability near a global bifurcation. Int J Bifurcation Chaos 2008;18(6):1759–65.
[47] Huang C. Multiple scales scheme for bifurcation in a delayed extended van der Pol oscillator. Physica A 2018;490:643–52.
[48] Auerbach D, Cvitanović P, Eckmann JP, Gunaratne G, Procaccia I. Exploring chaotic motion through periodic orbits. Phys Rev Lett 1987;58(23):2387–9.
[49] Eastham MSP. The spectral theory of periodic differential equations. Scottish Academy Press; 1973.
[50] Just W, Reibold E, Kacperski K, Fronczak P, Holyst JA, Benner H. Influence of stable floquet exponents on time-delayed feedback control. Phys Rev E 2000;61(5):5045–56.
[51] Costa DDA, Savi MA. Chaos control of an SMA–pendulum system using thermal actuation with extended time-delayed feedback approach. Nonlinear Dynam 2018;93(2):571–83.